Journal of Geophysical Research: Space Physics

RESEARCH ARTICLE
10.1029/2018JA025889

Ions Accelerated by Sounder-Plasma Interaction as Observed by Mars Express

A. Voshchepynets[1], S. Barabash[1], R. Ramstad[1], M. Holmstrom[1], D. Andrews[2], G. Nicolaou[1,3], R. A. Frahm[4], A. Kopf[5], and D. Gurnett[5]

[1]Swedish Institute of Space Physics, Kiruna, Sweden, [2]Swedish Institute of Space Physics, Uppsala, Sweden, [3]Department of Space and Climate Physics, University College London, London, UK, [4]Southwest Research Institute, San Antonio, TX, USA, [5]Department of Physics and Astronomy, The University of Iowa, Iowa City, IA, USA

Key Points:
- Accelerated ions are detected by IMA of ASPERA-3 during sounding phase of MARSIS radar
- The energy of accelerated ions is found to be in a range of 20 to 800 eV
- Observations coincide in time with periods when MARSIS transmits close to the plasma frequency

Correspondence to:
A. Voshchepynets,
woschep@gmail.com

Citation:
Voshchepynets, A., Barabash, S., Ramstad, R., Hölmstrom, M., Andrews, D., Nicolaou, G., et al. (2018). Ions accelerated by sounder-plasma interaction as observed by Mars Express. *Journal of Geophysical Research: Space Physics*, *123*, 9802–9814. https://doi.org/10.1029/2018JA025889

Received 11 JUL 2018
Accepted 6 NOV 2018
Accepted article online 10 NOV 2018
Published online 22 NOV 2018

Abstract The ion sensor of the Analyzer of Space Plasmas and Energetic Atoms (ASPERA-3) experiment detects accelerated ions during pulses of radio emissions from the powerful topside sounder: the Mars Advanced Radar for Subsurface and Ionosphere Sounding (MARSIS) onboard Mars Express. Accelerated ions (O_2^+, O^+, and lighter ions) are observed in an energy range up to 800 eV when MARSIS transmits at a frequency close to the plasma frequency. Individual observations consist of almost monoenergetic ion beams aligned with the MARSIS antenna or lying in the plane perpendicular to the antenna. The observed ion beams are often accompanied by a small decrease in the electron flux observed by the electron sensor of Analyzer of Space Plasmas and Energetic Atoms 3. Observations indicate that the voltage applied to the antenna causes charging of the spacecraft to several hundreds of volts by the electrons of the ambient plasma. Positively charged ions are accelerated when the spacecraft discharges.

1. Introduction

Operation of active wave devices in space, such as high-frequency transmitters in plasma, leads to a strong modification of the surrounding environment. Research in this domain has a long history and was initiated by experiments with rocket-based antennas back in the 1960s (Getmantsev & Denisov, 1962; Whale, 1964). Early studies (Benson, 1982; Laframboise et al., 1975; Oya, 1971, 1978; Shkarofsky, 1972) showed that intense radio frequency (RF) emission from an antenna may cause heating and acceleration of the local plasma. Shortly after, the first experimental evidence of such particles were found by Galperin et al. (1981) and James (1983) based on Interkosmos 19 and ISIS-1 and ISIS-2 observations, respectively. Galperin et al. (1981) reported on the existence of 100- to 500-eV electrons energized by 133-μs pulses from the sounder's transmitter on the spacecraft. In turn, James (1983), reported that 100-μs emission from the powerful sounder (nominal peak power 400 W) onboard the ISIS satellite results in acceleration of both electrons and ions to energies up to several hundreds of electron volts.

In the early study of Oya (1971) it was pointed out that the radiating power of the satellite-borne transmitter is such that the high-frequency energy density in the vicinity of the satellite is comparable with the thermal energy of the electrons. This implies that nonlinear effects such as wave-wave and wave-particle interactions of multiple resonances should be taken in to account. Weak turbulence models consider energization of the surrounding plasma by the interaction with cyclotron waves (Oya, 1971) and nonlinear Landau damping (Benson, 1982; Kiwamoto & Benson, 1979). The situation of the wave energy density from RF emission greatly exceeding the thermal energy of the electrons was later considered in the framework of strong turbulent models (Degtyarev et al., 1979). The collapse of Langmuir solitons, stimulated by the modulational (Pulinets & Selegei, 1986) or parametric instabilities (Serov et al., 1985), was shown to be an effective mechanism for electron heating in the vicinity of the transmitter. Acceleration/heating of ions could be caused by Landau damping of ion-acoustic waves stimulated by the modulational instability (Shuiskaia et al., 1990). Collapse of the plasma waves in the presence of a strong magnetic field has been considered by Krasnoselskikh and Sotnikov (1977). All models suggest that the energization of the surrounding plasma is stronger when the frequency of the transmitter matches one of the main plasma resonances: the electron plasma frequency f_{pe}, the upper hybrid frequency f_{UH}, the electron gyrofrequency f_{ce}, and/or its harmonics $n \cdot f_{ce}$ ($n = 2, 3, \dots$). Predictions are in good agreement with observations made by Intercosmos 19 (Galperin et al., 1981),

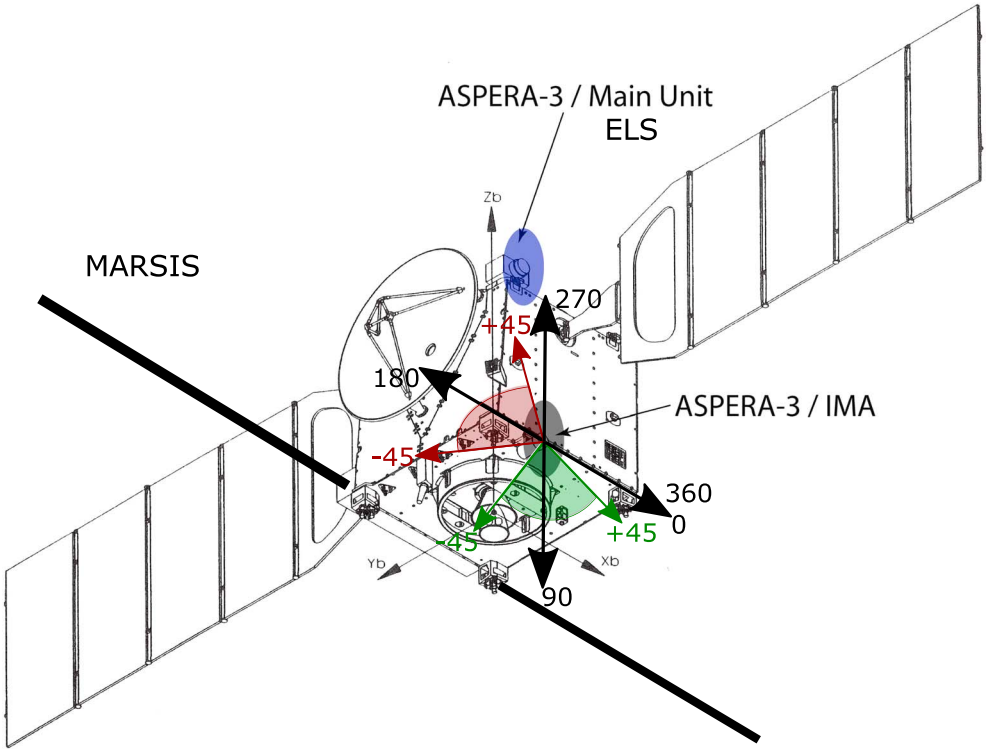

Figure 1. Accommodation of IMA, ELS, and MARSIS onboard MEX. Gray area shows the IMA field of view for 0° elevation (*XZ* plane). Red area shows viewing angles for 180° azimuth, and red arrows indicate ±45° elevation angles. Green area shows viewing angles for 90° azimuth, and green arrows indicate ±45° elevation angles. The total IMA field of view is 360° × 90°. Blue area shows schematically the 360° × 4° ELS field of view when scanner is parked at 90° position. For 0° scanner position the ELS field of view lies in the *YZ* plane. The *X* and *Z* axes are drawn as black arrows, with the +*Z* direction toward the local nadir (labeled 270). +*X* direction is labeled 0/360, and *Y* axis completes the right-handed coordinate system. IMA = Ion Mass Analyzer; ELS = Electron Spectrometer; MARSIS = Mars Advanced Radar for Subsurface and Ionosphere Sounding; MEX = Mars Express; ASPERA = Analyzer of Space Plasmas and Energetic Atoms.

ISIS-1 and ISIS-2 (James, 1987), and Cosmos-1809 (Shuiskaia et al., 1990). The most intense fluxes (up to 10^8 particles/eV/s/cm^2/str) of the nonthermal electrons and ions with energies up to 1 keV were detected by on-board particle spectrometers when the sounder frequency was around f_{pe}, f_{ce}, and $2f_{ce}$. Later, results obtained during the OEDIPUS C mission (Huang et al., 2001; James et al., 1999) showed that the electrons could be accelerated to energies above 20 keV and that the flux rates of terrestrial sounder-accelerated electrons are comparable to the intensities of spontaneous auroral fluxes.

Until recently, experimental studies of sounder-accelerated particles (SAP) were confined by conditions of Earth's ionosphere (Huang et al., 2001; James et al., 1999). Data collected by the Analyzer of Space Plasmas and Energetic Atoms (APERA-3) experiment (Barabash et al., 2006) onboard the Mars Express (MEX) spacecraft reveals somewhat similar phenomenon in the Martian ionosphere. Intense fluxes (up to 10^6 particles/eV/s/cm^2/str) of accelerated ions were detected by the Ion Mass Analyzer (IMA) shortly after the start of transmission from the topside sounder, the Mars Advanced Radar for Subsurface and Ionosphere Sounding (MARSIS) experiment (Gurnett et al., 2005; Picardi et al., 2004). SAP (mainly O^+ and O_2^+ ions) are frequently observed near pericenter when MARSIS is operational in its ionospheric mode. In this mode the MARSIS transmitter sends RF pulses of 91-μs duration, sweeping from 0.1 to 5.5 MHz (Jordan et al., 2009). From 2007 to 2016 MARSIS operated in ionospheric sounding mode on 3,771 orbits at altitudes below 1,000 km. IMA data are available only for 2,768 of those orbits, and 2,528 (91%) orbits were found to exhibit SAP. For the present study, 30 orbits were selected that are characterized by similar near Mars environment conditions. This provides sufficient statistics to investigate the physics of the phenomenon.

Studies of SAP observed by MEX can improve understanding of the plasma behavior in the near field of an active antenna in the Martian ionosphere. Detecting SAP will allow MEX to improve plasma diagnostics.

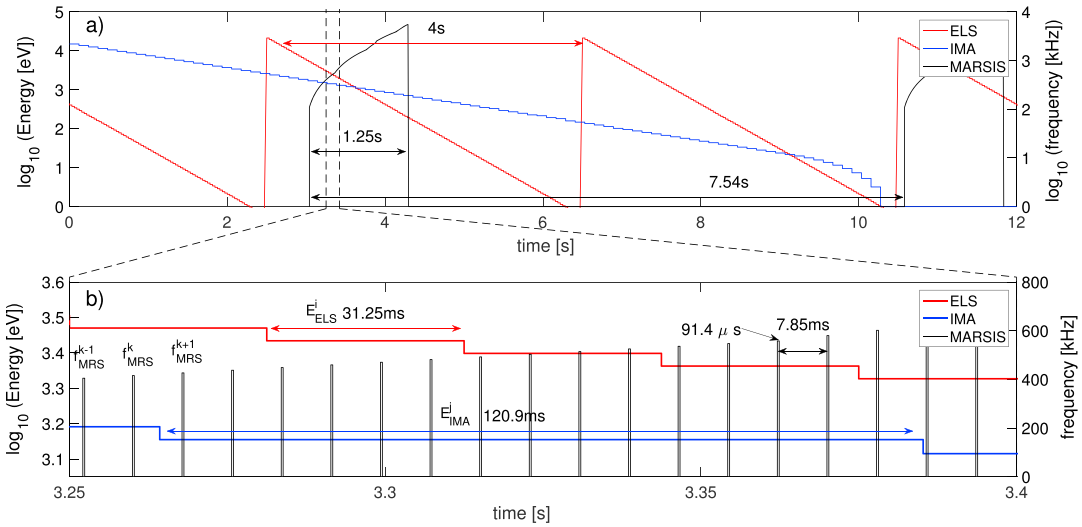

Figure 2. Timing of IMA (shown with blue line), ELS (shown with red line), and MARSIS (shown with black line). (a) Full energy scan of IMA takes 12 s. During the scan, IMA measures ions with energies from 36 keV down to 10 eV over 96 logarithmically equidistant steps. ELS measures electrons in 26-keV to 0.4-eV range sampled in 128 energy steps. Full energy scan is complete in 4 s. Active sounding phase of MARSIS lasts 1.257 s. During this phase, MARSIS sends 160 pulses with tone frequency from 0.1 to 5.5 MHz. Then instrument goes dead for 6.285 s, giving a repetition time of 7.54 s. (b) Sampling times of IMA and ELS are 120.8 and 31.25 ms, respectively. Duration of the each of MARSIS pulses is 91 μs. A pulse is followed by the ~ 7.312 ms of data collection time. The stepping time between pulses is ~ 7.855 ms. IMA = Ion Mass Analyzer; ELS = Electron Spectrometer; MARSIS = Mars Advanced Radar for Subsurface and Ionosphere Sounding.

2. Instruments

IMA provides ion measurements in the energy range 10 eV to 36 keV/q for the main ion components H^+, He^{++}, He^+, and O^+, and the group of molecular ions 20–80 amu/q. The mass per charge is determined by combining energy measurements from top hat electrostatic analyzer with velocity measurements from magnetic deflection system. For a given energy, ions of different velocity (or mass) hit different ring anodes of a large diameter microchannel plate. In total, the circular microchannel plate is divided into 32 ring (mass) anodes and 16 sectors given the arrival azimuth. IMA is mounted on the $-Z$ side of the spacecraft, with its axis pointed in the spacecraft $-Y$ direction (Figure 1). It has a 360° field of view in the spacecraft XZ plane, which is covered by 16 azimuthal sectors of 22.5°. In addition, IMA utilizes an electrostatic entrance deflection system to collect particles from within a region about ±45° in elevation which is perpendicular to the viewing plane of the instrument (also covered by 16 sectors in the elevation direction). For the time periods used in this work, the spacecraft velocity is in the YZ plane, within ±10° from the $+Y$ axis and $+Z$ points to local nadir.

The Electron Spectrometer (ELS) of Analyzer of Space Plasmas and Energetic Atoms 3 provides electron measurements in the energy range from 0.4 eV to 26 keV. In its survey mode, energy steps are logarithmically sampled in 128 channels, with an 8% energy resolution. The ELS 360° × 4° field of view is divided into 16 azimuthal sectors 22.5° each. ELS is located on a scanning platform. For the time periods used in this study the scanner was off and the ELS field of view was fixed. The ELS bore-plane was close (scanner is parked at 10°) to the YZ plane.

MARSIS is a low- to high-frequency, nadir-looking sounder that operates between 1.3 and 5.5 MHz in free space for subsurface sounding and between 0.1 and 5.5 MHz (wavelengths between 3000 and 55 m) for ionospheric sounding. Its 40-m dipole antenna is mounted on the opposite side of MEX with respect to IMA, and it is parallel to the X axis (Figure 1). The peak power output capability is 400 W (Jordan et al., 2009). The RF voltage magnitude that is applied to the transmitter is roughly 400 V, though it varies with frequency. Near antenna resonance, the voltage reduces, but the radiated power still remains high and roughly consistent with other frequencies. The actual voltage is ultimately set by the impedance of the antenna. MEX has nothing on board that can perform this measurement directly; however, it is assumed that the antenna impedance (and thus voltage) does not change significantly.

Figure 2 shows the timing of the IMA and ELS measurements along with the MARSIS transmission cycle. The IMA sampling time is 120.9 ms per step. One full 96-step energy scan takes 12 s including settle time for ion optics high voltage. The ELS sampling time is 31.25 ms of which 28.125 ms are accumulation and 3.125 ms are

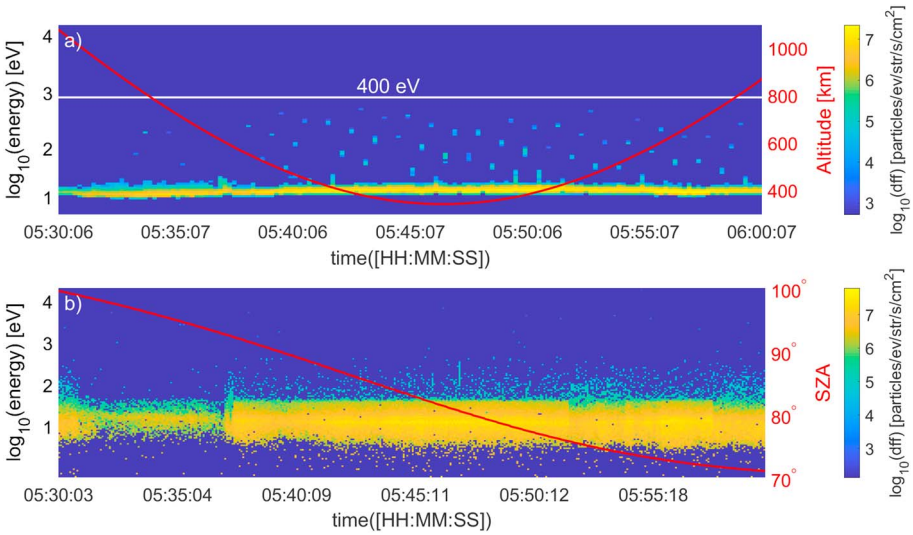

Figure 3. Data obtained by ELS and IMA sensors on 31 October 2013 from 05:30 to 06:0 4UTC. ELS data are sampled over 4 s, IMA data are sampled over 12 s. (a) O^+ differential number flux (dff [particles/eV/s/cm^2/str]); Mars Express altitude is superimposed and shown with red color; (b) electron dff superimposed with solar zenith angle (SZA). ELS = Electron Spectrometer; IMA = Ion Mass Analyzer.

latency. One full 128-step energy scan takes 4 s. During ionospheric sounding, the MARSIS sends a 91-μs pulse at a fixed frequency followed by 7.312-ms interval for listening and 0.45-ms interval of dead time. The frequency sweep takes 1.257 s to complete the 0.1- to 5.5-MHz range. After the frequency sweep has completed, the instrument remains quiet for 6.285 s, giving a repetition time of 7.54 s. The starting time of IMA and ELS measurements are not synchronized with the MARSIS transmission cycle. As a result, MARSIS can transmit up to 16 pulses within the 120.9 ms required for the IMA sampling time and up to 4 pulses during the ELS sampling time (Figure 2b). On the larger time scale, IMA can complete measurements over 10 consecutive energy channels during one MARSIS frequency sweep, while ELS can complete measurements over 40 consecutive channels within the same period of time (Figure 2a).

3. Observations

The present study focuses on O^+ ions because O^+ ions are the most abundant ion type in Martian ionosphere at altitudes higher than 300 km (Carlsson et al., 2006). Figure 3a shows the IMA O^+, and Figure 3b shows the ELS electron differential number fluxes (dff) in units of (particles/eV/s/cm^2/str) during 30 min around pericenter on orbit 12495 (pericenter reached at 31 October 2013 05:46:31 UTC). The MEX altitude and solar zenith angle are superimposed on the same panels and are shown with red color. To calculate dff fluxes shown in Figure 3, data have been collected from all available directions (for details on plasma moments and fluxes calculations see Fränz et al., 2006; Nilsson et al., 2012). The measurements shown in Figure 3 are typical for an undisturbed Martian ionosphere (Nilsson et al., 2012; Ramstad et al., 2015). At the altitudes under 1,000 km unperturbed O^+ ions are represented by a cold population with thermal energy less than 2 eV and peak flux around $1.5 \cdot 10^7$ particles/eV/s/cm^2/str. At the same time ELS measurements show electrons distributed in the energy range from 10 to 50 eV with peak flux around $3 \cdot 10^7$ particles/eV/s/cm^2/str. Intense periodic disturbances in ion data were detected by IMA when MEX altitude was below 1,000 km (Figure 3a). Each individual event is a group of accelerated O^+ ions observed in two to four consecutive energy channels of IMA, which indicates almost monoenergetic beams with $\Delta E/E_m$ about 10%, where ΔE is energy spread of the beam and E_m is mean beam energy. The beams are observed with energies starting from several tens of electron volts (typically 40 eV) but never exceeding 800 eV (limit is shown with the white line in Figure 3a). Corresponding differential fluxes are found to be lying within the range $10^4 - 10^5$ particles/eV/s/cm^2/str.

Detailed timing analysis has shown that the appearance of accelerated ions coincides with periods when MARSIS is transmitting. The time between two consecutive observations of accelerated ions is found to be 15, 23, 38, and 60 s that coincides with 2, 3, 5, 8 MARSIS repetition times. This could be clearly seen in Figure 4a. For illustration purpose the 9-min interval from 05:42:00 to 05:51:00 was chosen and only IMA measurements

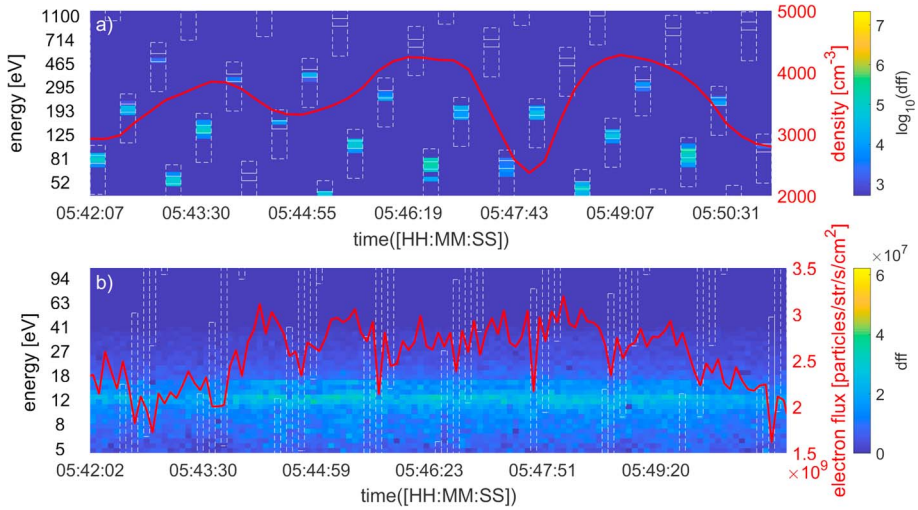

Figure 4. Data obtained by the Analyzer of Space Plasmas and Energetic Atoms 3 IMA and ELS on 31 October 2013. (a) Zoomed-in time interval of O^+ from 05:42:00 to 05:51:00; the 1.257-s intervals of the MARSIS active sounding phase are shown with white boxes. White lines within the boxes indicate those IMA measurements that have been done when MARSIS was operating in the range of frequencies from f_{pe} to $2f_{pe}$. Background plasma density measured by MARSIS is shown with red. (b) Zoomed-in time interval for electrons overlaid with the total flux of electrons, for energies up to 110 eV shown with a red line. The white boxes indicate ELS measurements made during 1.257 s of the MARSIS active sounding period. Sizes of the white boxes in panels (a) and (b) are different due to different time scales (Figure 2). IMA = Ion Mass Analyzer; ELS = Electron Spectrometer; MARSIS = Mars Advanced Radar for Subsurface and Ionosphere Sounding.

collected in the energy range from 40 to 1100 eV were considered. White boxes indicate the measurements that has been done during 1.257 s of the MARSIS active sounding phase. Intense fluxes of accelerated ions are only detected during these periods, shortly after MARSIS starts transmission.

In addition to remote radio sounding of the Mars ionosphere, MARSIS performs in situ measurements of the electron density (Andrews et al., 2013; Duru et al., 2008; Gurnett et al., 2005). Strong emission at harmonics of the local plasma frequency is produced in response to the transmission of the sounding pulse. The emission is received by the antenna enabling estimations of the electron density in the vicinity of the spacecraft once per $\sim$ 7.5 s. The plasma density is shown with the red line in Figure 4a. The measured density lies within the range from $3 \cdot 10^3$ to $4 \cdot 10^3$ cm^{-3} with the peak value obtained in the vicinity of the pericenter. Knowledge of the local plasma frequency enables the study of how the appearance of the accelerated ions is related to the frequencies of the MARSIS induced emission. During one IMA sampling period, MARSIS transmits 16 pulses with different frequencies. For this reason we can only define a range of MARSIS frequencies when ion acceleration is observed. Solid white lines within white boxes shown in Figure 4a indicate time intervals within $\sim$ 1.25-s periods of the MARSIS active sounding phase, when MARSIS transmits in the frequency range from f_{pe} to $2f_{pe}$. The peak flux of accelerated ions in each of the individual events matches these intervals. Beams with E_m below 200 eV are detected by IMA in four to five consecutive energy channels that corresponds to a wider range of MARSIS frequencies. During these 500–600 ms accelerated ions are detected by IMA before MARSIS starts transmission at the plasma frequency and are still observed even after the transmitting frequency has exceeded $2f_{pe}$. On the contrary, the typical time of the observations for the particles with mean energy higher than 200 eV is only 100–200 ms. These particles are observed when MARSIS operates in the range of frequencies close to $2f_{pe}$.

IMA has a much wider field of view in comparison to the instruments used in the previous studies. This enabled carrying out more detailed studies on directionality of the SAP fluxes with respect to the spacecraft. Typical time of the SAP observation is about 15–20 min per orbit. During this time IMA completes five to six full angular scans giving us only a few observations of SAP events per azimuth-elevation sector. In order to increase the number of observations, we combined data from 30 similar MEX orbits. The orbits were chosen to have altitude and location similar to the pass shown in Figure 3. Plasma conditions, such as electron and ion temperatures and electron plasma frequency, were close to those shown in Figure 3. These data were then used for all studies of the SAP characteristics presented below. Figure 5 shows a map of the angular locations in

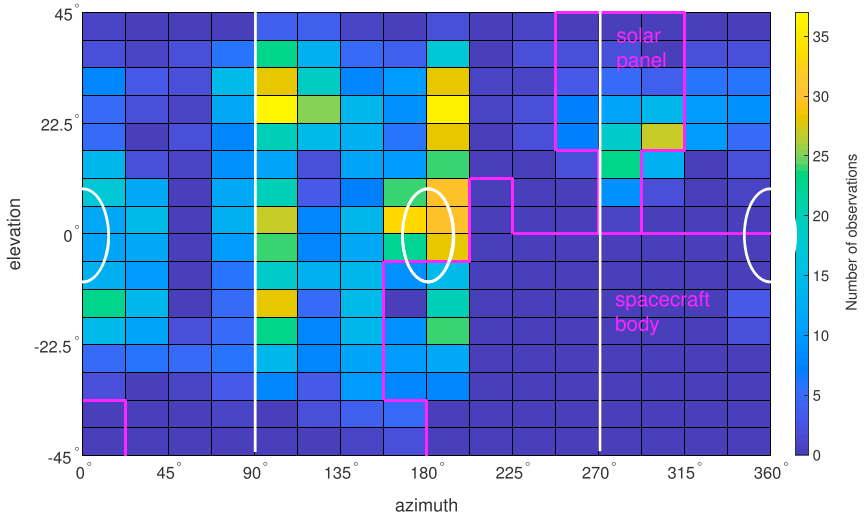

Figure 5. Spatial distributions of fluxes caused by SAP in the IMA field of view. The color shows the number of SAP events per IMA directional bin, corresponding to the IMA angular resolution. The white vertical lines show the plane perpendicular to the MARSIS antenna. The white ellipses indicate the direction around the MARSIS antenna of a ±10° cone. The area blocked by the spacecraft body is identified by the red lines. SAP = sounder-accelerated particles; IMA = Ion Mass Analyzer; MARSIS = Mars Advanced Radar for Subsurface and Ionosphere Sounding.

the IMA field of view where SAP events occur. It shows that the angular distribution of the ion fluxes is highly anisotropic. The majority of the particles were detected coming from direction that is aligned with the MARSIS antenna. This correspond to the azimuth angles near 180° and elevation angles around 0° (shown with the white ellipses). Two additional notable peaks are shifted in the elevation plane to about 25° and −20° along the 180° azimuth direction. The accelerated ions are also often detected in the plane perpendicular to the MARSIS antenna (azimuth angles 90° and 270°, shown with white lines). For azimuth angles close to 90° three distinct peaks could be seen at elevation angles $\sim -15°$, $\sim 0°$, and $\sim 25°$. As for azimuth angles close to 270°, only one peak is present for elevation angles of 20–25°. Due to obstruction of the IMA field of view by the spacecraft no accelerated particles were detected for azimuth angles above 200° and elevation angles below 0°. An additional obstacle for elevation angles above 0° is the solar panel; nevertheless, SAP are

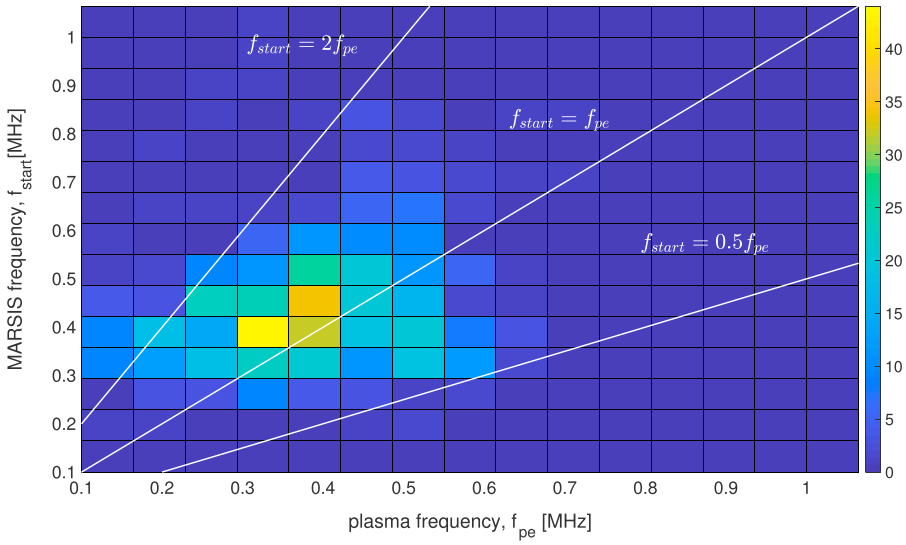

Figure 6. Number of sounder-accelerated particle events as a function of plasma frequency, f_{pe} (x axis), and Mars Advanced Radar for Subsurface and Ionosphere Sounding (MARSIS) frequency, f_{start} (y axis). White lines represent linear relationships $f_{start} = 0.5f_{pe}$, $f_{start} = f_{pe}$, and $f_{start} = 2f_{pe}$.

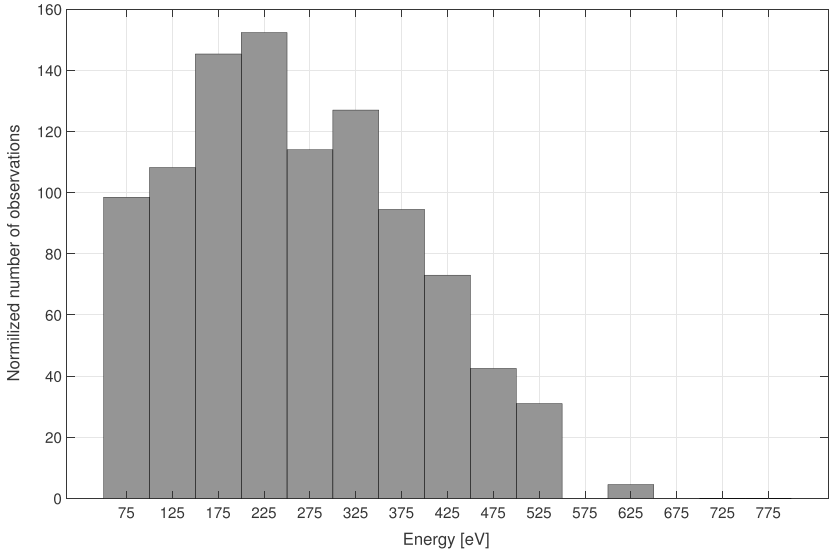

Figure 7. Number of SAP observations as a function of the SAP energy. The number of observation within a certain energy range was averaged by the number of Ion Mass Analyzer energy channels that correspond to this energy range. SAP = sounder-accelerated particles.

frequently detected coming from that direction. A plausible reason is that due to the rotation of the solar array, its actual orientation may not fully occupy the outline marked in Figure 5.

As it was mentioned before, not all of the pulses within the MARSIS frequency sweep result in acceleration of the ions. Only after the MARSIS frequency of RF emission exceeds a certain limit SAP are observed. In order to define this limit, we have selected the first observation in each of individual events where SAP occurred and then took the mean value of MARSIS frequencies, f_{start}, that correspond to this observation. The number of SAP events as a function of both f_{start} and f_{pe} is shown in Figure 6. The highest number of observations corresponds to $f_{start} \sim 400$ kHz, while 80% of the total number of observations occurred when f_{start} was within the range from 300 to 500 kHz. Very similar results were obtained for the distribution of the plasma frequency. The maximum number of SAP observations corresponds to $f_{pe} \sim 400$ kHz and that coincides with the corresponding maximum for f_{start}. The distribution of f_{pe} is slightly more dispersed then the distribution of f_{start}, where 80% of the total number of observations correspond to a wider range of frequencies, that is, 250–550 kHz. Comparison of f_{start} and f_{pe} showed a linear dependence of f_{start} on f_{pe}. The majority of the observations correspond to the area slightly above the line $f_{pe} = f_{start}$ (showed with the white line); and thus, one may conclude that ion acceleration becomes efficient when the frequency of MARSIS transmission slightly exceeds the plasma frequency. A similar analysis made in order to determine the upper frequency limit events shows that SAP rapidly decreases after the frequency of MARSIS transmission exceeds $2f_{pe}$.

The acceleration process cannot be considered as constant even on time scales of the acquisition time because the efficiency of the ion acceleration depends on the emission frequency. Due to these reasons it is not possible to study the energy spectrum of accelerated particles without making additional assumptions. In order to avoid this, our study was focused on how often SAP are observed within a certain energy range. The results are shown in Figure 7. For each event of SAP the energy that corresponds to the highest flux was selected. SAP fluxes detected simultaneously coming from different directions were considered as separate events.

Energies of SAP were found to be within the range from 50 to 650 eV, with a majority of the observations detected in the energy range between 150 and 350 eV. Observations of the ions with higher energies are quite rare; for instance, the number of observations of SAP with energies above 400 eV is only 10% of the total number of observations. The highest number of observation corresponds to the energy range from 200 to 250 eV. Observations of the ions with energies near 800 eV are very rare, and we excluded these observations from the present analysis due to the statistics of a low count rate (of the order of the noise level). The 50 eV lower-energy limit is not firm, as periodic disturbances in ion fluxes between 20 and 50 eV caused by MARSIS

RF pulses are frequently observed by IMA. Apart from SAP, this energy range is also populated by thermal ions at low altitudes and it is not always possible to make a clear distinction between the two populations.

4. Discussion

Contrary to Earth, Mars has no strong intrinsic magnetic field. Far from the regions with strong crustal magnetic field, typical magnitude of the magnetic field in the Martian ionosphere at the altitudes above several hundreds kilometers is below tens of nanoteslas. Absence of the strong magnetic field can be a reason why SAP electrons are rarely observed by ELS, while accelerated ions are frequently detected when MARSIS operates in ionospheric sounding mode at the altitudes below 1,000 km. Studies of the SAP electrons in the Earth ionosphere (Galperin et al., 1981; James, 1983) showed that the SAP electrons are primarily detected when frequency of the transmitter matches electron gyrofrequency, f_{ce} or its harmonic, or when it lies in the range of the diffuse resonances (Oya, 1971; Shuiskaia et al., 1990). At the gyroresonance, electrons can be heated/accelerated due to the Landau damping of the radio wave, while in the diffuse resonance region (between harmonics of the electron gyrofrequency) electrons can be heated by electron-cyclotron waves exited by the RF emission in the vicinity of the antenna. Recently, electron acceleration by an active antenna in collisionless plasma has been studied by means of particle-in-cell (PIC) simulations (Dieckmann et al., 2004). The study showed the electrons can be effectively accelerated in the very near field of antenna when the frequency of the transmitter is equal to the first harmonic of the electron gyrofrequency. Because magnetic field in the Martian ionosphere is weak, MARSIS almost always operates in a regime where the frequency of the sending pulses far exceeds the local electron gyrofrequency. Since the frequency of the RF emission is far from the discussed resonances, it cannot effectively accelerate/heat local electrons. That can explain the lack of SAP electrons detection by ELS.

SAP ions are typically detected when the frequency of the transmitter is close to the local plasma frequency. As pointed out by Galperin et al. (1981), wave energy density of the emitted RF wave, W, can be much higher than the plasma thermal pressure, n_eT_e, in the vicinity of the antenna. Under this condition, RF emission can cause development of the modulational instability which leads to the formation of plasma cavities where the wave energy condenses. The collapse of these cavities leads to a dissipation of the RF field by the Landau damping mechanism, resulting in acceleration of electrons and ions. Analysis of the data collected by the wide-band high-frequency analyzer 2 onboard Interkosmos 19 carried out by Pulinets and Selegei (1986) supports this model. The authors showed that intensity and duration of the plasma response to the sounder pulse, measured by high-frequency analyzer 2 on the local plasma frequency, are in agreement with predictions from the model based on collapsing solitons. Also, it was shown that time delay between the start of the pulse and plasma response coincides with the characteristic time of the modulational instability development. The authors suggested that electrons are accelerated due to the Landau damping of the Langmuir waves that are generated during collapse (Degtyarev et al., 1979; Pulinets & Selegei, 1986). Further study (Shuiskaia et al., 1990) showed that damping of the ion-acoustic waves generated by the modulational instability can cause ion heating of the ionospheric plasma near the satellite.

Wave energy density in the near the zone of a long cylindrical source can be estimated as follows:

$$W = \frac{Pf_{RF}}{2\pi rcL\sqrt{f_{RF}^2 - f_{pe}^2}}. \quad (1)$$

Here we considered the case when the frequency of the transmitted wave, f_{RF}, is higher than the local plasma frequency, f_{pe}, that corresponds to the observations of the SAP ions by IMA (for the details of the case $f_{RF} < f_{pe}$, we refer to Pulinets & Selegei, 1986). In equation (1) we used the following notations: W = wave energy density, P = transmitted power, L = length of the antenna, c = speed of light, and r = distance in the direction perpendicular to the antenna. One can use the equation (1) to estimate the characteristic scale on which wave energy exceeds the plasma thermal pressure, $W \geq n_eT_e$, as follows:

$$r_p = \frac{Pf_{RF}}{2\pi n_eT_ecL\sqrt{f_{RF}^2 - f_{pe}^2}}, \quad (2)$$

here n_e and T_e are the electron density and temperature, respectively. Figure 8a shows r_p as a function of MARSIS frequency calculated for the conditions typical for MEX: $P = 20$ W, $L = 40$ m, $n_e = 3 \cdot 10^3$ cm^{-3}, $T_e = 1$

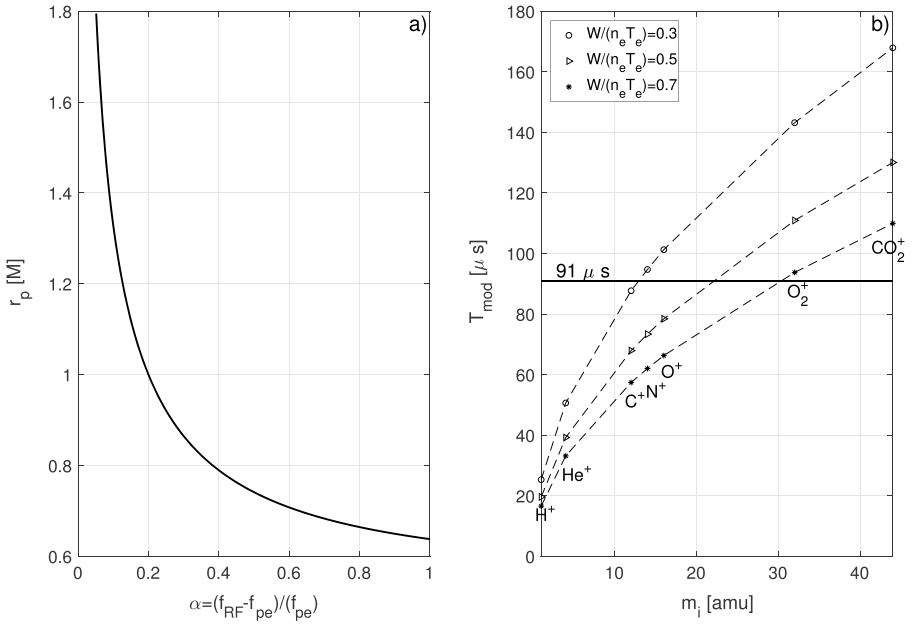

Figure 8. (a) Characteristic scale of the turbulence, r_p, as a function of the MARSIS frequency. (b) Characteristic time of the growth of the modulational instability as function of the main ion constituent in the plasma. Solid black line indicates duration of the MARSIS pulse. Different symbols correspond to a different W/n_eT_e ratios: circle = 0.3, triangle = 0.5, and dot = 0.7. MARSIS = Mars Advanced Radar for Subsurface and Ionosphere Sounding.

eV, $f_{pe} \sim 500$ kHz, f_{RF} starts with 525 kHz and runs up to 1,000 kHz. For the frequencies close to the plasma frequency we obtain $r_p \approx 1.8$ m. The scale decreases with increasing frequency of the transmitter and for $f_{RF} = 2f_{pe}$, r_p is only slightly above 60 cm, which is very close to the asymptotic solution of $r_p \approx 55$ cm for $f_{RF} \gg f_{pe}$. It is worth noting that distance between MARSIS and IMA is more than 2 m, and thus, ion measurements should not be strongly affected by high-frequency pressure of the RF waves.

In general, condition required for the modulational instability to develop is $W/(n_eT_e) > m_e/m_i$, where m_e and m_i are masses of electron and ion, respectively. If this condition is satisfied the characteristic time of growth of the instability, T_{mod}, can be estimated as follows (Pulinets & Selegei, 1986):

$$T_{mod} = \frac{1}{2\pi f_{pe}} \left(\frac{W}{n_eT_e} \frac{m_e}{m_i} \right)^{-1/2} \tag{3}$$

According to the results of the numerical simulations (Degtyarev et al., 1979), the mechanism of soliton formation is effective for small W/n_eT_e ratios with saturation at $W \sim 0.5 n_eT_e$. Figure 8a shows characteristic time of the growth, T_{mod}, of the modulational instability estimated for different W/n_eT_e ratios: 0.3, 0.5, and 0.7. Such level of turbulence is expected at distances from 1.5 m (for $W/n_eT_e = 0.7$) to 3.5 m (for $W/n_eT_e = 0.1$) from the antenna, when MARSIS frequency is ~ 700 kHz. As one can see, in case of oxygen plasma, T_{mod} is below a limit of 91 μs (show with solid black line), and thus, duration of a MARSIS pulse is long enough for solitons to form. The lifetime of the solitons is of the order of l_c/c_s, where l_c is the size of the soliton and $c_s^2 \sim T_e/m_i$ is the ion sound velocity. Collapse of the solitons is accompanied by the radiation of ion-acoustic waves, which are subject to a strong Landau damping if $T_e \approx T_i$. Damping of the ions-acoustic waves results in acceleration of the ions in the electric field of these waves.

Landau resonance occurs when the velocity of a particle is very close to the phase velocity of the waves, $2\pi f/k$, here f and k are frequency and wave-vector of the wave. For the ion-acoustic wave

$$v_{ph}^2 = \frac{4\pi^2 f^2}{k^2} = \frac{T_e}{m_i} \frac{1}{1 + k^2 \lambda_D^2}, \tag{4}$$

where λ_D is Debye length. In case of modulational instability driven by a bumping wave with wave-vector $k_0 = 2\pi f_0/c$, the solitons occur in the region of k space with

$$k_s = k_0 \left(\frac{m_e}{m_i} \frac{W}{n_eT_e} \right)^{1/2}. \tag{5}$$

Results of numerical simulations (Degtyarev et al., 1979) showed that a maximum of acoustic and Langmuir spectra take place at $k > k_s$. Taking k_s as a lower limit for the acoustic spectrum (development of the turbulence runs toward smaller scales, that implies larger k), one can estimate upper limit of the phase-space occupied by ion-acoustic waves:

$$v_{\max}^2 = \frac{T_e}{m_i} \frac{1}{1 + k_0^2 \lambda_D^2 \left(\frac{m_e}{m_i} \frac{W}{n_e T_e} \right)} \tag{6}$$

For the conditions mentioned above, $v_{\max}$ is approximately equal to the ion sound velocity. This sets an upper limit for the velocity that can be reached by the ions. In this case, an increase in the energy of the ions is equal to a difference between electron and ion temperatures, $\Delta E = T_e - T_i$. For typical conditions at Mars, the proposed mechanism can explain ion acceleration up to energy of several tens of electron volts, while SAP ions detected by IMA have energies up to 800 eV. It is worth noting that PIC simulations showed formation of a hot electron sheath in the vicinity of an antenna (Dieckmann et al., 2004). The sheath can be dense enough to support strong waves that can produce high-energy electrons and ions.

In order to explain observations of SAP ions on the ISIS-2 spacecraft, James (1983) proposed a model based on the assumption that the negative satellite direct current (DC) potential is built up on the spacecraft during an RF pulse. For the frequencies up to f_{pe}, the difference in electron and ion mobility causes a rectification effect and results in a negative DC potential on the spacecraft. As the frequency of the RF emission increases above f_{pe}, the amplitude of electron motion in electric field of antenna decreases. This in turn leads to a reduction of electron current collected by the antenna/spacecraft. If the frequency of the RF pulse significantly exceeds plasma frequency, $f_{RF} \gg f_{pe}$, electrons cannot provide effective charging of the antenna or spacecraft. The model suggests that a steady negative DC potential on the order of the voltage applied to the antenna (V_0) is built up on the spacecraft when the transmitter is on. This implies that the instantaneous potential of the antenna with respect to the plasma oscillates from ~ 0 to $-2V_0$ (for more details we refer to Figure 7 in James, 1987). The ions with the highest energy can be detected during this period. After the end of the applied RF pulse, the antenna-spacecraft system is discharged by the ion current. Decay of the DC potential during the discharge phase results in a down sweep in the detected ion energy. This model explained some of the characteristics of the ion fluxes measured by soft particle spectrometer onboard the ISIS-2 spacecraft. Later, analysis of the data collected by the Cylindrical Electrostatic Probe onboard ISIS-2 provided additional evidence of the existence of the negative DC potential on the spacecraft (James, 1987).

Observations of SAP by IMA onboard MEX are in agreement with this model of spacecraft charging. Following James (1983), one can estimate the characteristic time of charging, τ_e, for MARSIS/MEX system as follows:

$$\tau_e = \frac{4V_0}{n_e v_{te} A (1 + \frac{eV_0}{k_B T_e})} \cdot \frac{\pi \epsilon_0 l}{\ln(\frac{l}{R}) - 1} \tag{7}$$

v_{te} is the electron thermal velocity. The parameters A and l correspond to the surface area of the MARSIS antenna and its half length, $R = \sqrt{(a^2 + b^2)/2}$, here a and b are semimajor and semiminor axis of the elliptical cross section of the antenna. Constants e, ϵ_0, and k_B are the electron charge, vacuum permittivity, and Boltzmann constant. The first fraction on the right-hand side of the equation (7) corresponds to the resistance, R_s, associated with the electron-saturation current, I_s, that is, $R_s = V_0/I_s$. The second fraction on the right-hand side of equation (7) is the antenna capacitance estimated in the vacuum limit, C_a; and thus, $\tau_e = R_s \cdot C_a$. Substituting the corresponding antenna characteristics ($l = 20$ m, $a = 19$ mm, $b = 8$ mm, $V_0 = 400$ V) and assuming reasonable values for electron density and temperature ($n_e = 3 \cdot 10^3$ cm^{-3} and $T_e = 1$ eV) one can get $\tau_e = 12$μs. The estimated charging time is shorter than duration of one MARSIS pulse, $t_M = 91$μs, which implies that electrons have enough time to build up a negative potential on the spacecraft. On the other hand, due to the higher mass, the lower mobility ions cannot discharge the system effectively on such a small time scale. Assuming simplified plasma conditions, $T_e = T_i$ and $n_e = n_i$ (where T_i and n_i are the ion temperature and density, respectively), the characteristic time for discharging by the ion current can be estimated as $\tau_i = \sqrt{(m_i/m_e)}\tau_e$. Even in the case of hydrogen plasma ($\sqrt{(m_i/m_e)} \sim 42$), the characteristic time $\tau_i \sim 500$μs is much longer than the period of a MARSIS pulse. More accurate estimation for O^+ ions with density $n_i = n_e/2$ results in $\tau_i = 4.1$ ms. This result indicates that the antenna-spacecraft system can be discharged by the ion current generated by the negative potential within the $\sim$ 7.76-ms interval between two consecutive MARSIS pulses.

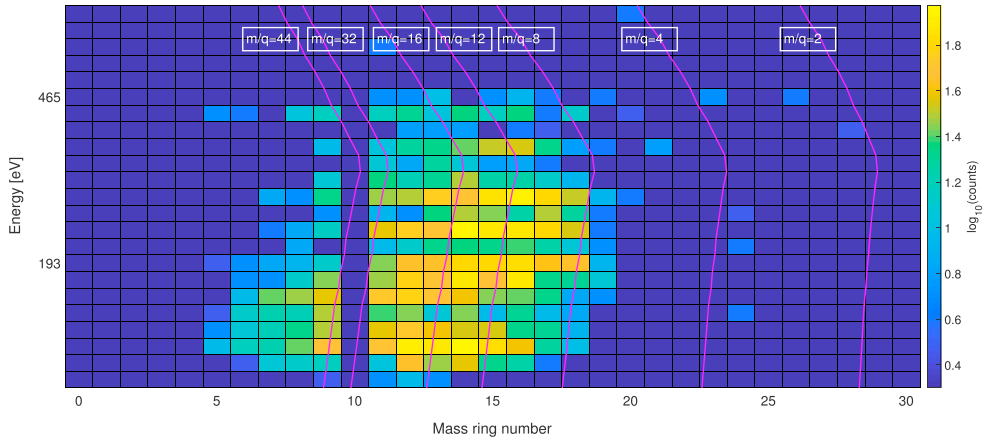

Figure 9. Analyzer of Space Plasmas and Energetic Atoms 3 Ion Mass Analyzer energy/mass matrix obtained during events of sounder-accelerated particles on 31 October 2013 05:30 to 06:04 UTC. The vertical axis represents the energy per charge in electron volts, and the horizontal axis represents the mass ring number. Overplotted are the expected mass lines for ions with different mass/charge ratio. (Note: Mass ring 10 removed due to uncertain calibration.)

The proposed model explains some of the characteristics of the accelerated ions observed by IMA. For instance, the upper limit of the energy of detected particles was found to be 800 eV, which coincides with a doubled value of the potential on the antenna. Observations show that fluxes of the accelerated ions from a lower-energy range are more intense than the fluxes of more energetic ions (Figures 3a and 4a). Partially, this might be caused by a large difference in the duration of time between intervals when particles with different energies could be detected. According to the model, ions with energies from 400 to 800 eV could be observed only within the $t_M - \tau_e \sim$ 79-μs interval between the moment when potential around spacecraft is already set up by the end of the RF pulse. Particles with lower energies could also be detected during the much longer discharge phase. The fact that the peak of the ion energy distribution was found to be 225 eV might indicate that the charging process occurs far less effective than estimated by equation (7) and the DC potential built up on the spacecraft at the end of the MARSIS pulse is usually on the order of −225 V. Ions with energies above 225 eV are assumed to be accelerated during the RF pulse while electrons with lower energies are mainly accelerated during the discharge phase. In this case the highest energy that can be reached by ions during the RF pulse is limited to 625 eV.

Analysis of the data collected by ELS indicates the presence of the negative potential around the spacecraft. Figure 4b shows the electron differential flux measured during the period when the most intense fluxes of accelerated ions were detected. The total flux of electrons with energies up to 110 eV is shown with a red line. As before, the white boxes denote time intervals on which MARSIS is turned on. One may notice that the electron flux measured during these periods is considerably lower in comparison to measurements that were made when MARSIS was idle. The decrease in electron flux are caused by the negative potential that lasts several ms after the end of the RF pulse and prevents electrons from entering ELS.

5. Possible Application

Acceleration of the charged particles by powerful RF sounders might be used for conducting new types of active experiments in space. One of the possible applications is the active diagnostic of plasma. Acceleration of the ions in an induced electric potential implies that the lighter ions will be accelerated to higher energies during the recharging phase. This effect is illustrated by Figure 9. This figure shows the energy-mass matrix accumulated by the IMA during events of SAP during the orbit 12495 together with theoretical mass lines for ions with different mass-to-charge ratios (lighter particles correspond to higher mass ring number). Figure 9 shows that the position of the mass peak shifts toward higher mass ring numbers as energy of the ions increases. The reason why lighter ions are accelerated to the higher energy is due to the higher mobility of these ions, which can reach spacecraft surface sooner. Negative potential decreases with time as the ions current discharges the spacecraft; and thus, ions that come later in time have lower energies. This effect might be used for detection of the ion species that constitute minor fractions in the surrounding plasma. For instance, a mass peak that corresponds to $m/q = 8$ could be clearly seen at the energy ~420 eV, while under

normal conditions ($E_m \sim 20$eV) it is quite hard to identify this type of ion. Although this effect can potentially enable us to measure ions that are difficult to observe under normal ionospheric conditions, correct interpretation of these measurements requires information about the electric potential on the whole spacecraft. Significant negative potential induced on the spacecraft during RF pulse will not only strongly affect the energy of detected ions but also particle trajectories in the vicinity of the spacecraft. As a result, determination of the initial directions and energies of the ions will be very complicated task. Future numerical simulations of the charging and discharging phases of the spacecraft under plasma conditions close to those in the Martian ionosphere are required. As it was shown by Dieckmann et al. (2004) PIC simulations can be used as a practical tool to examine SAP related phenomena.

6. Summary

Data collected by IMA onboard MEX enabled a study of the effect of charged particles acceleration in the vicinity of a powerful RF transmitter under plasma conditions other than that of the Earth's ionosphere. The study showed that the intense fluxes of SAP (ions up to 10^6 particles/eV/s/cm^2/str) are frequently observed during periods when MARSIS operates in the range of frequencies from f_{pe} to $2f_{pe}$. Observation of the accelerated ions is often accompanied by a decrease in electron flux detected by ELS. Ions from SAP have typical energy ranges up to 550–800 eV. A model for the RF-induced spacecraft potential (James, 1983) suggests that ions at the highest energies are collected during the 91-μs RF field, while lower-energy ions are collected during the few millisecond discharge period following the pulse. The orientation of fluxes from SAP is found to be often aligned with MARSIS antenna or lying in the plane perpendicular to its dipole.

The creation of substantial charged particle fluxes by RF transmitters has important implications for active experiments in space physics. For instance, injection of artificially created beams of energetic electrons is a well-known technique for remote diagnostics of space plasma (Paschmann et al., 2001). In addition, there are evidences that sounder-accelerated electrons can produce optical (Gough et al., 2009) and radio (James, 2004) emission. Active diagnostic of the plasma composition can serve as an another example of such experiments. A combination of the electric potential that decreases with time and time-of-flight effect results in acceleration of the lighter particles to higher energy, enabling identification of the ions species that are almost indistinguishable under normal conditions. This could be used to improve upon our knowledge of the ion composition of the Martian ionosphere.

Acknowledgments
Data used in this study are available on the NASA Planetary Data System, via http://pds-geosciences.wustl.edu/missions/mars_express/aspera.htm. The ASPERA-3 experiment on the ESA MEX mission is a joint effort between 15 laboratories in 10 countries, all sponsored by their national agencies. We thank all of these agencies as well as the various departments/institutions hosting these efforts. In particular we wish to acknowledge support through the Swedish National Space Agency to the PI institution in Sweden dnr. 169/15 and the National Aeronautics and Space Administration (NASA) in the United States under NASA contract NASW-00003 at Southwest Research Institute. A.V. is grateful to H. G. James for important comments.

References

Andrews, D. J., Opgenoorth, H. J., Edberg, N. J. T., André, M., Fränz, M., Dubinin, E., et al. (2013). Determination of local plasma densities with the MARSIS radar: Asymmetries in the high altitude Martian ionosphere. *Journal of Geophysical Research: Space Physics*, *118*, 6228–6242. https://doi.org/10.1002/jgra.50593

Barabash, S., Lundin, R., Andersson, H., Brinkfeldt, K., Grigoriev, A., Gunell, H., et al. (2006). The Analyzer of Space Plasmas and Energetic Atoms (ASPERA-3) for the Mars Express mission. *Space Science Reviews*, *126*, 113–164. https://doi.org/10.1007/s11214-006-9124-8

Benson, R. F. (1982). Stimulated plasma instability and nonlinear phenomena in the ionosphere. *Radio Science*, *17*(6), 1637–1659. https://doi.org/10.1029/RS017i006p01637

Carlsson, E., Fedorov, A., Barabash, S., Budnik, E., Grigoriev, A., Gunell, H., et al. (2006). Mass composition of the escaping plasma at Mars. *Icarus*, *182*, 320–328. https://doi.org/10.1016/j.icarus.2005.09.020

Degtyarev, L. M., Solovev, G., Shapiro, V. D., & Shevchenko, V. I. (1979). Formation of fast-electron tails in a strong Langmuir turbulence. *Soviet Journal of Experimental and Theoretical Physics Letters*, *29*, 543–549. https://doi.org/10.1029/2004JA010436

Dieckmann, M. E., Rowlands, G., Eliasson, B., & Shukla, P. K. (2004). Particle-in-cell simulations of electron acceleration by a simple capacitative antenna in collisionless plasma. *Journal of Geophysical Research*, *109*, A12304. https://doi.org/10.1029/2004JA010436

Duru, F., Gurnett, D. A., Morgan, D. D., Modolo, R., Nagy, A. F., & Najib, D. (2008). Electron densities in the upper ionosphere of Mars from the excitation of electron plasma oscillations. *Journal of Geophysical Research*, *113*, A07302. https://doi.org/10.1029/2008JA013073

Galperin, I. I., Sagdeev, R. Z., Shuiskaia, F. K., Lisakov, I. V., Migulin, V. V., Kushnerevskii, I. V., et al. (1981). Detection of electron acceleration in the ionospheric plasma under the influence of high-power radio radiation near the local plasma frequency aboard the space vehicle Interkosmos 19. *Cosmic Research*, *19*, 34–44.

Getmantsev, C. G., & Denisov, N. G. (1962). Concerning an effect during measurement of electron concentration in the ionosphere by the antenna probe method. *Geomagnetism and Aeronomy*, *2*, 575.

Gough, M. P., Hardy, D. A., & James, H. G. (2009). First results from the energetic particle instrument on the OEDIPUS-c sounding rocket. *Advances in Space Research*, *21*, 705–708. https://doi.org/10.1016/S0273-1177(97)01008-9

Gurnett, D. A., Kirchner, D. L., Huff, R. L., Morgan, D. D., Persoon, A. M., Averkamp, T. F., et al. (2005). Radar soundings of the ionosphere of Mars. *Science*, *310*, 1929–1933. https://doi.org/10.1126/science.1121868

Huang, C. Y., Burke, W. J., Hardy, D. A., Gough, M. P., James, H. G., Villalón, E., & Gentile, L. C. (2001). Electron acceleration by megahertz waves during OEDIPUS C. *Journal of Geophysical Research*, *106*(A2), 1835–1848. https://doi.org/10.1029/1999JA000286

James, H. G. (1983). Sounder-accelerated particles observed on ISIS. *Journal of Geophysical Research*, *88*(A5), 4027–4040. https://doi.org/10.1029/JA088iA05p04027

James, H. G. (1987). Discharge of RF-induced spacecraft dc potential by positive ions. *Planetary Space Science*, *35*, 105–118. https://doi.org/10.1016/0032-0633(87)90149-8

James, H. G. (2004). Slow Z-mode radiation from sounder-accelerated electrons. *Journal of Atmospheric and Solar-Terrestrial Physics*, *66*, 1755–1765. https://doi.org/10.1016/j.jastp.2004.07.035

James, H. G., Sotnikov, V. I., Burke, W. J., & Huang, C. Y. (1999). OEDIPUS-C observations of electrons accelerated by radio frequency fields at whistler-mode frequencies. *Physics of Plasmas*, *6*, 4058–4069. https://doi.org/10.1063/1.873668

Jordan, R., Picardi, G., Plaut, J., Wheeler, K., Kirchner, D., Safaeinili, A., et al. (2009). The Mars express MARSIS sounder instrument. *Planetary Space Science*, *57*, 1975–1986. https://doi.org/10.1016/j.pss.2009.09.016

Kiwamoto, Y., & Benson, R. F. (1979). Nonlinear Landau damping in the ionosphere. *Journal of Geophysical Research*, *84*, 4165–4174. https://doi.org/10.1029/JA084iA08p04165

Krasnoselskikh, V., & Sotnikov, V. (1977). Plasma-wave collapse in a magnetic field. *Soviet Journal of Plasma Physics*, *3*, 872–879.

Laframboise, J. G., Rubinstein, J., & Palmer, F. H. (1975). Theory of topside sounder transmission effects on antenna quasistatic sheath impedance. *Radio Science*, *10*(8-9), 773–784. https://doi.org/10.1029/RS010i008p00773

Fränz, M., Dubinin, E., Roussos, E., Woch, J., Winningham, J. D., Frahm, R., et al. (2006). Plasma moments in the environment of Mars. Mars express ASPERA-3 observations. *Space Science Reviews*, *126*, 165–207. https://doi.org/10.1007/s11214-006-9115-9

Nilsson, H., Stenberg, G., Futaana, Y., Holmström, M., Barabash, S., Lundin, R., et al. (2012). Ion distributions in the vicinity of Mars: Signatures of heating and acceleration processes. *Earth, Planets and Space*, *64*, 135–148. https://doi.org/10.5047/eps.2011.04.011

Oya, H. (1971). Verification of theory on weak turbulence relating to the sequence of diffuse plasma resonances in space. *Physics of Fluids*, *14*, 2487–2499. https://doi.org/10.1063/1.1693358

Oya, H. (1978). Generation mechanism of proton cyclotron echoes due to pulsed radio frequency waves in space plasma. *Journal of Geophysical Research*, *83*(A5), 1991–2008. https://doi.org/10.1029/JA083iA05p01991

Paschmann, G., Quinn, J. M., Torbert, R. B., Vaith, H., McIlwain, C. E., Haerendel, G., et al. (2001). The Electron Drift Instrument on Cluster: Overview of first results. *Annales Geophysicae*, *19*, 1273–1288. https://doi.org/10.5194/angeo-19-1273-2001

Picardi, G., Biccari, D., Seu, R., Marinangeli, L., Johnson, W. T. K., Jordan, R. L., et al. (2004). Performance and surface scattering models for the Mars Advanced Radar for Subsurface and Ionosphere Sounding (MARSIS). *Planetary Space Science*, *52*, 149–156. https://doi.org/10.1016/j.pss.2003.08.020

Pulinets, S. A., & Selegei, V. V. (1986). Ionospheric plasma modification in the vicinity of a spacecraft by powerful radio pulses in topside sounding. *Journal of Atmospheric and Terrestrial Physics*, *48*, 149–157. https://doi.org/10.1016/0021-9169(86)90079-6

Ramstad, R., Barabash, S., Futaana, Y., Nilsson, H., Wang, X.-D., & Holmström, M. (2015). The Martian atmospheric ion escape rate dependence on solar wind and solar EUV conditions: 1 Seven years of Mars Express observations. *Journal of Geophysical Research: Planets*, *120*, 1298–1309. https://doi.org/10.1002/2015JE004816

Serov, A. A., Galperin, I. I., Lisakov, I. V., & Shuiskaia, F. K. (1985). Local acceleration of electrons of a near-satellite plasma by radio emission from a high-power onboard transmitter. *Kosmicheskie Issledovaniia*, *23*, 431–443.

Shkarofsky, I. P. (1972). Nonlinear sheath admittance, currents, and charges associated with high peak voltage drive on a VLF/ELF dipole antenna moving in the ionosphere. *Radio Science*, *7*(4), 503–523. https://doi.org/10.1029/RS007i004p00503

Shuiskaia, F. K., Gal'Perin, I. I., Serov, A. A., Baranets, N. V., & Kushnerevskii, I. V. (1990). Resonant heating of the ionospheric plasma by powerful radiopulses aboard the Intercosmos-19 and Cosmos-1809 satellites. *Planetary Space Science*, *38*, 173–180. https://doi.org/10.1016/0032-0633(90)90081-Z

Whale, H. A. (1964). Ion sheath effects near antennas radiating within the ionosphere. *Journal of Geophysical Research*, *69*(3), 447–455. https://doi.org/10.1029/JZ069i003p00447